HHS Public Access

Author manuscript

Ultrasound Med Biol. Author manuscript; available in PMC 2024 August 01.

Published in final edited form as:

Ultrasound Med Biol. 2023 August ; 49(8): 1719–1727. doi:10.1016/j.ultrasmedbio.2023.03.016.

Evaluation of Myocardial Stiffness in Cardiac Amyloidosis Using Acoustic Radiation Force Impulse and Natural Shear Wave Imaging

Felix Q. Jin[a,*], **Vaibhav Kakkad, Ph.D.**[a,*], **David P. Bradway, Ph.D.**[a,*], **Melissa LeFevre**[b], **Joseph Kisslo, M.D.**[b], **Michel G. Khouri, M.D.**[b], **Gregg E. Trahey, Ph.D.**[a,c]

[a:]Department of Biomedical Engineering, Duke University, Durham, North Carolina, USA;

[b:]Department of Cardiology, Duke University Medical Center, Durham, North Carolina, USA;

[c:]Department of Radiology, Duke University Medical Center, Durham, North Carolina, USA

Abstract

Objectives: Increased myocardial stiffness (MS) is an important hallmark of cardiac amyloidosis (CA) caused by myocardial amyloid deposition. Standard echocardiography metrics assess MS indirectly via downstream effects of cardiac stiffening. The ultrasound elastography methods Acoustic Radiation Force Impulse (ARFI) and natural shear wave (NSW) imaging assess MS more directly.

Methods: This study compared MS in twelve healthy volunteers and thirteen patients with confirmed CA using ARFI and NSW imaging. Parasternal long-axis acquisitions of the interventricular septum were obtained using a modified ACUSON Sequoia scanner and a 5V1 transducer. ARFI-induced displacements were measured through the cardiac cycle, and ratios of diastolic-over-systolic displacement were calculated. NSW speeds from aortic valve closure were extracted from echocardiographic-tracked displacement data.

Results: ARFI stiffness ratios were significantly lower in CA patients than controls (mean ± sd of 1.47 ± 0.27 vs. 2.10 ± 0.47; $p < 0.001$), and NSW speeds were significantly higher in CA patients than controls (5.58 ± 1.10 m/s vs. 3.79 ± 1.10 m/s; $p < 0.001$). A linear combination of the two metrics demonstrated greater diagnostic potential than either metric alone (AUC = 0.97 vs 0.89 and 0.88).

Conclusions: MS was measured to be significantly higher in CA patients using both ARFI and NSW imaging. Together, these methods show potential utility to aid in clinical diagnosis of diastolic dysfunction and infiltrative cardiomyopathies.

Corresponding Author: Vaibhav Kakkad (v.kakkad@duke.edu), Duke University Pratt School of Engineering. Room 1427, Fitzpatrick Center (FCIEMAS), 101 Science Drive, Campus Box 90281, Durham, NC 27708-0281, Phone: (919) 660-5131, Fax: (919) 684-4488, Twitter: @dukeultrasound.

*These authors contributed equally

Keywords

acoustic radiation force; amyloidosis; echocardiography; elastography; myocardial stiffness; natural shear waves

Introduction

Cardiac amyloidosis (CA) is a restrictive cardiomyopathy resulting from the deposition of amyloid fibrils and consequent remodeling within the myocardial interstitium. CA can rapidly progress to life-threatening heart failure within five years following diagnosis [1]. Early diagnosis of CA is required to effectively leverage attenuated heart failure morbidity and mortality outcomes afforded by recent advances in disease-specific pharmacologic treatments [2]. Non-biopsy diagnosis of transthyretin (ATTR) cardiac amyloidosis through cardiac magnetic resonance and nuclear scintigraphy has increased detection [3,4]; however, CA remains underdiagnosed with diagnostic delays and advanced stage presentations still common [5]. Given the recent development of highly effective, albeit expensive, therapeutic options for ATTR-CA, namely the approval of tafamidis as well as the ongoing trials for patisiran, vutrisiran, eplontersen, and NTLA-2001, there is substantial interest in finding cost-effective and accessible diagnostic tests to facilitate early and accurate identification of patients suspected to have CA [6,7]. Compared to magnetic resonance and nuclear imaging, ultrasound-based imaging is more accessible, less expensive, and does not require ionizing radiation or contrast agents. However, conventional echocardiographic parameters have relatively poor sensitivity and specificity for CA [8]. Thus, there remains an unmet clinical need for a reliable and specific ultrasound-based metric for the detection and diagnosis of CA.

The historical gold standard for measuring global myocardial stiffness (MS) is the pressure-volume loop, but ultrasound-based techniques have shown potential to noninvasively measure MS throughout the cardiac cycle in a localized manner. Ultrasound elastography techniques measure soft tissue elasticity (i.e., stiffness) and have been proposed for assessing differences in MS associated with pathology, including CA. Proposed approaches include external vibration [9], tracking naturally-occurring shear waves generated by valve closure or the atrial kick [10–12], and calculating tissue strain over the cardiac cycle [13,14]. A recent study that examined natural shear wave (NSW) speeds and global longitudinal strain found increased MS in patients with CA compared to healthy volunteers (HVs) [15].

Acoustic radiation force impulse (ARFI) and shear wave elasticity imaging (SWEI) are ultrasound elastography techniques that measure transient mechanical responses to assess tissue stiffness. In these methods, a pulse of high-intensity ultrasound is used to induce micron-scale tissue displacements. In ARFI imaging, on-axis displacements are tracked, whereas in SWEI, the resultant mechanical shear waves are tracked laterally as they propagate away from the point of mechanical excitation (“push”), with the goal of estimating the apparent wave speed. Stiffer regions of tissue exhibit smaller on-axis displacements and faster wave speeds relative to more compliant regions. Feasibility studies

have shown positive results using ARFI and SWEI to noninvasively measure MS in human subjects [16–25].

Measurement of MS through a combination of ARF-based methods and NSW-based elastography could help better characterize myocardial mechanical properties and consequently better inform therapeutic decision-making, not only for CA, but also for other cardiac pathologies such as aortic stenosis and mitral regurgitation, hypertrophic cardiomyopathy [26], myocarditis [27], and infiltrative diseases like hemochromatosis [28]. This study was designed to determine the feasibility and potential of combining ARFI and NSW imaging to differentiate myocardial stiffness in CA patients from that in HVs. We evaluated both individual and combined diagnostic performances of these stiffness quantification methods and compared their relationships with existing echocardiography metrics in our study population.

Materials and Methods

Study Design and Population:

This prospective study was conducted at Duke University Medical Center's Cardiac Diagnostic Unit (CDU) and was approved by the Duke University Medical Center Institutional Review Board (IRB) (Protocol Pro00032068). No patient health information was recorded prior to written informed consent.

Twelve HVs and thirteen patients with confirmed CA were enrolled in the study. Both groups were age-restricted to 50 years or older. CA was confirmed by a combination of typical features on cardiac imaging (magnetic resonance, echocardiography) and biopsy, or nuclear scintigraphy (technetium pyrophosphate scan) with negative monoclonal protein assessments. Twelve CA patients had the ATTR subtype and were used for subsequent analysis. Enrollment for the study occurred in 2019. After imaging, some of the subjects were involved in a placebo-controlled amyloid clinical trial at the time. Three of the amyloid subjects were also on patisiran, which is a treatment for neuropathy in amyloid.

The primary eligibility criteria were: patients with confirmed cardiac amyloidosis and healthy volunteers with no history of cardiovascular disease (e.g., hypertension, diabetes, and conduction/structural abnormalities), medical therapy potentially influencing cardiac function (e.g., chemotherapy), or surgical procedures potentially affecting transthoracic imaging windows. All controls had normal left ventricular (LV) ejection fraction (EF) ≥55%. Individuals with pacemakers or other implants and those receiving intravenous contrast were excluded to avoid potential risks associated with the acoustic and thermal output of the longer ultrasound pulse lengths employed in the ARFI imaging sequences. Subjects were not screened based on transthoracic echocardiographic (TTE) image quality in previous or current clinical exams nor on BMI. In the outpatient setting, individuals who met the primary eligibility criteria were introduced to the study by IRB-approved CDU personnel prior to their scheduled echocardiogram.

Standard Echocardiography:

In this study, an ACUSON Sequoia ultrasound system (Siemens Medical Solutions USA, Inc., Issaquah WA) was used to perform both the clinical exam and study scan. Acoustic output measurements were performed to ensure the scanner met Food and Drug Administration (FDA) guidelines for patient exposure (mechanical and thermal indices, see Appendix A).

Following informed consent and measurement of vital signs, a standard echocardiographic exam was performed using standard, unmodified B-mode, color and spectral Doppler imaging. Parasternal long axis (PLAX), parasternal short axis (PSAX), apical four chamber, apical two chamber, apical long axis, and subcostal views were obtained. Evidence of any valvular disease or arrhythmia were noted. Measurements to assess LV volumes and EF (calculated by Simpson's biplane method), right ventricular (RV) function, LV dimensions, LV mass and LA volume were performed according to recommendations for cardiac chamber quantification [29]. LV diastolic function was graded according to current guideline recommendations (normal grade 0 or abnormal grades 1 to 3) [29,30]. LV strain measurements were calculated and analyzed offline using IMAGE-ARENA version 4.6 (TOMTEC Imaging Systems GmbH, Unterschleissheim, Germany). Additional echocardiographic metrics were calculated for statistical comparisons: E/e', the ratio of early mitral inflow velocity to mitral annular early diastolic velocity, LA volume index (LAVi), the ratio of LA volume to body surface area, and the myocardial contraction fraction (MCF), the ratio of LV stroke volume to myocardial volume that was recently proposed for ATTR-CA [31].

Custom Ultrasound Sequences - Data Acquisition:

Through a research collaboration with Siemens Ultrasound, engineering-level access to the ACUSON Sequoia scanner was obtained, allowing both the modification of imaging mode pulse sequences and the acquisition of raw echocardiographic data. A custom sequence was developed for the 5V1 cardiac phased array, specially adapted for acquisition of ARFI and NSW acquisitions, with 50 repeated measurements at 20 Hz over multiple cardiac cycles, along a fixed line-of-sight transmit direction. Continuous pulse-inversion harmonic tracking pulses were transmitted at a pulse repetition frequency of 5 kHz. After each acquisition sequence, a 30-second waiting time was observed before the next acquisition. The 30 second pause was set based on a system technical limit and not directly a result of transducer face heating or ISPTA limits. Subjects were imaged in the supine or oblique positions. Concurrent electrocardiogram (ECG) was recorded for retrospective alignment to the cardiac cycle. The custom ultrasound sequence imaging protocol was completed following the standard echocardiographic exam and aimed at assessing the stiffness of the interventricular septum (IVS) in the PLAX and PSAX views. In each view, three ARFI acquisitions were recorded at each of three pulse durations, up to 800 μs. The scanner delivered these ARFI pulses focused at sonographer-selected focal depths in the range 4.75 – 8.75 cm. The entire aperture was used for all focal depths, so the F/# varied from 2.3 to 4.2 over the supported focal positions. The focal depths did not vary within the 50-push acquisition, but the focal lengths were sufficiently long to ensure displacement and tracking was achieved throughout the septum. The pulse amplitude was not varied with focal depth.

None of the scanner's built-in acoustic output calculations or limits for MI and TI were overridden. Following ARFI imaging, three repetitions of NSW tracking were acquired in each view. For all acquisitions, subjects were asked to hold breathing for ten seconds while each dataset was captured. The raw echocardiographic data were stored throughout the procedure and processed off-line using MATLAB 2019b software (MathWorks Inc., Natick, Massachusetts).

Processing and Analysis:

The raw echocardiographic imaging data were processed using a band-pass filter motion correction algorithm and correlation-based tracking methods to yield micron-level axial displacements (see Appendix B). Axial displacements were measured over a lateral extent of 1.5 mm for ARFI. M-mode representations of the raw echocardiographic data were used to identify the axial borders of the IVS over the cardiac cycle and isolate the displacement data within the IVS. For ARFI acquisitions, mean displacement over a complete cardiac cycle and previously identified metrics of data quality (such as contrast, temporal coherence, and spatial similarity) were used to exclude data points that were likely to be unreliable [17]. The details of this processing step, threshold values used, and rationale are provided in Appendix B.

As in our previous work [17], a metric termed the stiffness ratio was calculated from the mean ARFI displacement from diastole over that of systole. These phases of cardiac cycle were extracted from the segmented ECG signals which were acquired synchronously with the ultrasound acquisitions. Because the exact magnitude of the applied radiation force is unknown, a single ARFI displacement measurement at any one point in the cardiac cycle is not a quantitative measure of stiffness. However, when one divides the displacement measured during diastole by the displacement measured during systole, while assuming the applied force was the same, a pseudo-quantitative metric to grade MS can be calculated [17].

NSW speeds were calculated from PLAX measurements of particle motion data in the IVS over the cardiac cycle. The tracking sequence and motion estimation were the same as ARFI as discussed above in Appendix B. Particle velocity data were extracted at a depth centered over the IVS and over a lateral extent of 17.5 mm. NSW events were identified algorithmically by comparing peak particle velocities and ECG waveforms. Data were pre-processed with a 15–100 Hz bandpass filter, and then an automated radon-transform method [32] was used to estimate the NSW speeds, similar to previous studies [10,33]. NSW propagation was assumed to be along the IVS, but because displacements were tracked over a purely lateral segment, calculated speeds were corrected by $\cos(\theta_{tilt})$ to compensate for the tilt of the IVS. This angle was measured manually on the corresponding B-mode at the time of NSW occurrence. Tracking quality and identification of NSWs associated with mitral valve closure were poor, so the NSW speeds associated with aortic valve closure (AVC) were used for further analysis.

Statistical Analysis:

ATTR-CA and HV groups were compared using two-tailed, two sample t-tests for continuous variables. Continuous data for variables are displayed as mean ± standard

deviation. Comparisons with a p-value of 0.05 or lower were considered statistically significant for all tests. Correlations between the novel metrics (ARFI stiffness ratio and AVC NSW speed) and echocardiography metrics associated with CA (IVSd, E/e', GLS, LAVi, and MCF) were computed. For these comparisons, linear fits and R-value show the degree of correlation for each pair of metrics. Statistics were calculated using MATLAB 2019b software.

Results

Study Demographics:

Twenty-five subjects were enrolled in the study (12 HV and 13 CA). Among CA patients, 12 had transthyretin type (ATTR-CA), of which 10 were hereditary, of which eight had the p.V142I transthyretin gene mutation. Table 1 shows subject population characteristics. All healthy volunteers were in normal sinus rhythm, while seven of the 13 subjects in the CA group had atrial fibrillation.

Standard Echo Results:

Table 2 shows the standard echocardiographic exam parameters. There were statistically significant differences between the HV and ATTR-CA groups for clinical (age, BP, HR, BMI, etc.) and echocardiographic parameters (EF, wall thickness, strain and tissue Doppler imaging (TDI)).

ARFI Stiffness Ratio and NSW Speed:

Figure 1 illustrates representative B-mode, M-mode, and ARFI data comparing the HV and CA group. Qualitative differences can be observed in all three sets of data. In the B-mode and M-mode, the IVS appears thicker and demonstrates lower variability in width over the cardiac cycle for the CA patient relative to the HV. In the ARFI data, the HV shows not only higher peak diastolic displacement but also a substantially higher ratio of diastolic-to-systolic displacements. The trends highlighted in Figure 1 were consistently observed in the ARFI data across multiple heartbeats, acquisitions, and patients included in this analysis.

Figure 2 illustrates B-mode and NSW data comparing a representative HV and a CA patient. The B-mode, again, illustrates a morphological difference in myocardial structure, with a significantly thicker IVS in the CA patient. Yield of MVC was notably lower: from the 25 subjects in the study, we obtained 82 MVC measurements and 125 AVC measurements. There were 6 subjects without any MVC data versus 3 subjects without AVC data. In the parasternal acoustic window used for this study, the waves from the MVC event were less consistent and more difficult to track. Due to the better quality and reliability of AVC events in our data, AVC alone was used in analyses to grade MS. Average speeds for MVC and AVC events in healthy volunteers were 4.4 m/s and 3.8 m/s respectively and were not significantly different.

Of the 24 subjects analyzed in the study, 22 had measurable ARFI stiffness ratios and 21 had measurable NSW speeds, shown in Figure 3. The stiffness ratio was lower in ATTR-CA

patients than in HVs ($p < 0.001$), and the NSW speed was higher in ATTR-CA patients than in HVs ($p < 0.001$). Both lower ARFI stiffness ratio and faster NSW speed indicated greater diastolic MS.

Figure 3 also shows that ARFI stiffness ratios and NSW speeds were weakly correlated ($R = -0.41$). To increase diagnostic utility, we considered a composite metric, which we call the Myocardial Stiffness Index, by calculating a linear combination of the two metrics. We used the following formula: $NSW\_Speed - 2.78 * Stiffness\_Ratio$, where the respective weighting coefficient was inversely proportional to the observed standard deviation of observed data. This combined metric was statistically significantly higher in ATTR-CA patients than in HVs ($p < 0.0001$).

Correlations between Stiffness Ratio, NSW Speed, and Cardiac Echo Metrics:

Table 3 lists the correlation coefficients between the ARFI stiffness ratio, NSW speed, and cardiac echocardiographic metrics. Figure 4 shows the correlations between five CA-associated echocardiographic metrics and the stiffness ratio and NSW speed. Moderate correlation was observed between the stiffness ratio and IVSd, mean GLS, LAVi, and MCF, and between natural wave speed and IVSd, E/e', and MCF.

Diagnostic Utility of Stiffness Ratio and NSW Speed:

Figure 5 shows the ROC curves for using the stiffness ratio, the NSW speed, and the Myocardial Stiffness Index to discriminate between HVs and CA patients. Table 4 reports the sensitivity, specificity, and area under the ROC curve (AUC). We used bootstrapping by sampling with replacement to obtain 95% confidence intervals for the AUC values. Both stiffness ratio and NSW speed had good diagnostic utility, with an AUC of 0.89 and 0.88 respectively. Myocardial Stiffness Index, the combined metric, had an AUC of 0.97, higher than either metric alone.

Discussion

In recent years, ARFI, SWEI, and NSW-based stiffness measurement techniques have been proposed as noninvasive and low-cost ways for measuring MS to characterize underlying cardiac pathology and potentially differentiate between various etiologies of heart failure [26,34]. In this cross-sectional study, we found that ARFI stiffness ratio was lower and AVC-induced NSW speed was higher in ATTR-CA patients compared to HV controls. Our results corroborate previously reported findings concerning septal NSW speeds in CA patients. This work is the first application of the ARFI stiffness ratio to amyloidosis, demonstrating that ARFI alone or combined with NSW imaging are potential clinical tools for assessment of MS to aid in the diagnosis of diastolic dysfunction and infiltrative cardiomyopathies.

In CA, amyloid deposition in the myocardial interstitium results in thickened ventricular walls, elevated atrial pressures, and atrial dilation [35]. Existing echocardiographic parameters have low sensitivity and specificity for CA, with the most promising metrics being interventricular septal thickness, the E/e' ratio, the left atrial volume index [35], and the myocardial contraction fraction (MCF), which was recently explored for ATTR-

CA [31]. No echo parameters solely diagnose cardiac amyloidosis (CA), but rather only raise suspicion for the diagnosis. Further diagnostic testing with other imaging modalities or endomyocardial biopsy is needed to make the clinical diagnosis of cardiac amyloidosis in current practice. Besides IVS thickness as noted in our work, other clinical echocardiographic metrics which may separate the normal subjects from the cardiac amyloid subjects include TDI, strain, myocardial contraction fraction (MCF) and mass. Longitudinal strain has also been explored for CA, with preservation of LV strain at the apex relative to mid- and basal segments shown to be characteristic of CA as compared to other causes of ventricular hypertrophy. Strain metrics do not directly measure myocardial elasticity, but rather observe the functional consequences of amyloid deposition disrupting normal cardiomyocyte function [15,36–39].

ARFI and NSW imaging directly evaluate MS and provide a more mechanical perspective of the heart tissue. ARFI provides uncalibrated stiffness measurements through the entire cardiac cycle, and the stiffness ratio quantifies the degree of tissue stiffening between diastole and systole, which reflects baseline stiffness in a fully relaxed state and the efficiency of contraction. NSW elastography provides an absolute measure of stiffness but is constrained by both the location and timing of the NSWs associated with aortic valve closure (AVC), mitral valve closure (MVC), and the atrial kick. In this study, we were able to detect and measure at least one AVC wave in each patient; however, yield for MVC was much lower, so we chose to use AVC measurements for further analyses. We hypothesize that the more posterolateral source location of MVC waves may be one factor leading to worse yield. One study of NSWs in three dimensions revealed that a more complex wave propagation resulted from MVC due to its unique bicuspid geometry [40].

In comparing ARFI M-modes (Figure 1) and NSW data (Figure 2), we observed that AVC and MVC measurements often occur during transitions between contracted and relaxed myocardium. For example, AVC propagation through the septum typically occurred near the beginning of isovolumic relaxation. The resulting stiffness estimates are neither at peak mechanical systole or diastole, likely increasing variability and degrading predictive value. Because NSW imaging provides a snapshot of MS at a given time, and it may be considered in the future to use NSW measurements as a way to calibrate ARFI M-mode data.

The ARFI-based metric is the ratio between MS at diastole and systole. In contrast, the NSW speed is a more absolute measure of MS at a single time within the cardiac cycle. Because these two approaches probed different aspects of MS, we created the Myocardial Stiffness Index, a combined metric incorporating ARFI and NSW measures, to synthesize data from both elastography methods. While the Myocardial Stiffness Index was derived based on empirical evidence from data collected in this study alone, herein it was found to show stronger separation between CA and HV compared to the stiffness ratio or NSW speed individually.

ARF-induced SWEI may also be used to generate transient shear waves at other times in the cardiac cycle and locations in the myocardium, but accurate tracking of these shear waves is complicated by a variety of factors associated with cardiac morphology and mechanics (i.e., dispersive geometric effects [41]) and transthoracic ultrasound image quality [16,42]. We

initially intended to interrogate the feasibility of SWEI to characterize myocardial stiffness over the cardiac cycle; however, this analysis was excluded from the main results due to poor and inconsistent data quality. A detailed report of SWEI through the cardiac cycle and its sensitivity to image quality are presented in Appendix C.

Clinicians may wish to review the recorded echocardiographic data to determine acquisition quality. For ARFI stiffness ratio, the M-mode stiffness map (Figure 1) would help verify that displacements are tracked in the septum and have a periodicity aligning with the cardiac cycle. For NSW elastography, the plot of particle velocities (Figure 2) would help verify that a shear wave is observed and that the automatically-estimated wave trajectory aligns with the apparent wave.

In the present work, we observed slightly lower displacement ratios than previously reported [17] even in the HV group, perhaps due to the increased age of this cohort compared to our previously studied population. We noted that a number of metrics including interventricular septal thickness and average global longitudinal strain achieved 100% separation in our cohort. We attributed this to our small sample size and the manner in which we recruited clinically-diagnosed, advanced CA patients.

The thickness of the septum was on the order of the wavelength of a NSW. Therefore, we expected NSWs to propagate in a wave-guided regime. Indeed, the term “natural shear wave” is slightly misleading, as the wave is not a pure shear wave in a homogenous bulk material. Recent papers have acknowledged but mostly ignored this effect [34,43], and we used the NSW terminology to remain consistent with literature. Under a Lamb wave model, the wave velocity depends on both thickness and absolute shear modulus. Preliminary analysis of our data’s phase velocity curves showed that observed NSW speed differences between patients were not explained by differences in septal thickness, suggesting that measured NSW speeds reflected underlying stiffness and not simply septal thickness. In the future, a more detailed phase velocity analysis (see [44]) should be performed.

In this study, particle velocity was used to detect NSW due to higher signal quality; acceleration data was not used due to increased noise (see [33]). In the future, NSW speed reliability could be improved with longer acquisitions and by tracking displacements over 2-D regions.

Study Limitations:

This study was limited in the number of subjects we were able to enroll due to difficulties with scheduling of both the experimental equipment and personnel. Enrolled were 12 HV controls and 13 CA patients with advanced disease, of which 12 had ATTR-CA. These subjects exhibited marked ventricular thickening, severely enlarged left atria, decreased LVEF, and depressed longitudinal strain. The two groups had significant phenotypic differences which limited the clinical impact of differentiating them with the novel methods proposed.

Although the HV group was age limited to 50 years and up, age differences between the two groups remained. Age itself is a known determinant of myocardial stiffness, and this may

have partially confounded interpretation of differences between the two groups. A further study should enroll subjects in more tightly age-matched groups.

Only one sonographer and hospital were used in this feasibility study. Therefore, the relative diagnostic performance of the stiffness ratio, NSW speed, and echocardiographic metrics like IVSd may not have been representative of the larger population of interest. Future studies will be required to assess the relative performance of various imaging metrics for detecting and evaluating cardiac amyloidosis and other cardiomyopathies.

Subjects in the CA group with atrial fibrillation were not excluded from analysis and thus may have influenced the results. Arrhythmias complicated the analysis of beat-to-beat variability and R-R intervals, and they likely affected loading conditions and contractility in the heart. Arrhythmias also reduce our ability to detect NSWs induced by valve closure. As such, this cohort may differ from those of other cardiac diseases such as left ventricular hypertrophy due to hypertension, which may exhibit relatively fewer subjects with atrial fibrillation. This may also account for some discrepancies with other published studies which excluded subjects with arrhythmias [45].

Both cardiac ARFI and NSW imaging rely on making measurements through the available cardiac imaging windows. Both methods are limited in the angles and depths that can be used to place the tissue of interest at the right position and orientation in the imaging plane. The ROI for ARFI must be far enough away that clutter and ringdown does not obscure the tracking of the induced displacement, but not so far that the radiation force can generate a measurable displacement. Furthermore, each method gives only a partial view into the overall cardiac mechanics. ARFI only gives insight into the stiffness of the tissue under the push beam, while NSW tracking is only possible after a few cardiac events (atrial kick, aortic valve closure and mitral valve closure) and along specific directions within the appropriate chamber walls of the heart.

There also exists a need for a more robust evaluation of inter-acquisition and inter-session repeatability to identify and mitigate the impact of sources of variation that currently dilute diagnostic value. A more global assessment of myocardial stiffness would be helpful to understand the spatial trends across different walls of the heart and the temporal trends over the cardiac cycle. As a long-term goal, tools to aid in mapping the propagation of myocardial stiffness change over time could enable “cardiac elastophysiology”, an analogue to the way propagation of electrical changes is currently mapped over the cardiac cycle in cardiac electrophysiology.

Conclusions

This study demonstrated that measurements by ARFI and NSW elastography correlated with functional and morphological derangements due to cardiac amyloid infiltration, and that these metrics provided information unique from currently used echocardiographic measurements including speckle-tracking strain imaging. These results support the feasibility of further study toward integrating these noninvasive imaging methods into clinical practice utilizing a commercial-grade ultrasound scanner. Transthoracic ARFI

imaging and NSW elastography have potential utility as clinical tools to aid in the detection and monitoring of diastolic dysfunction and infiltrative cardiomyopathies.

Supplementary Material

Refer to Web version on PubMed Central for supplementary material.

Acknowledgements

The authors would like to thank Kristine Arges for assistance with the clinical protocol, Siemens Medical Solutions USA, Inc. for in-kind and technical support, Katelyn Flint, Ph.D. for acoustic output measurement and sequence development contributions, David Soriano and Tanvi Santosh for data collection and processing assistance, and Ned Danieley for computational infrastructure support. This research was supported by the National Heart, Lung, and Blood Institute through grant R37HL096023. Any opinions, findings, and conclusions or recommendations expressed in this material are those of the authors and do not necessarily reflect the views of the National Institutes of Health.

Conflict of Interest Statement

Joseph Kisslo is a speaker and consultant for Philips and GE. Michel Khouri reports research support from Pfizer, Alnylam Pharmaceuticals, Eidos Therapeutics, and Boston Scientific; consulting/advisory board support from Pfizer, Alnylam Pharmaceuticals, and Eidos Therapeutics, and is a member of Alnylam Pharmaceuticals Speaker's Bureau. Gregg E. Trahey reports a financial interest in Samsung Inc., which is developing products related to the research described in this paper; he has IP in Acoustic Radiation Force Impulse (ARFI) and shear wave elasticity imaging. His lab at Duke University has a master research agreement with Siemens Medical Solutions USA, Inc. In this work ARFI imaging is described in an implementation that is not FDA-cleared for clinical use. The other authors report no disclosures.

Data Availability Statement

The research data collected for use in this study are not suitable to post publicly, due to both proprietary, confidential Siemens Ultrasound scanner information as well as an omission of a data sharing clause in the IRB protocol under which the research study was conducted, Data not available / The data that has been used is confidential

Reference List

[1]. Connors LH, Sam F, Skinner M, Salinaro F, Sun F, Ruberg FL, et al. Heart Failure Resulting from Age-Related Cardiac Amyloid Disease Associated with Wild-Type Transthyretin: A Prospective, Observational Cohort Study. Circulation 2016;133:282–90. [PubMed: 26660282]

[2]. Maurer MS, Schwartz JH, Gundapaneni B, Elliott PM, Merlini G, Waddington-Cruz M, et al. Tafamidis Treatment for Patients with Transthyretin Amyloid Cardiomyopathy. N Engl J Med 2018;379:1007–16. [PubMed: 30145929]

[3]. Dorbala S, Ando Y, Bokhari S, Dispenzieri A, Falk RH, Ferrari VA, et al. ASNC/AHA/ASE/EANM/HFSA/ISA/SCMR/SNMMI Expert Consensus Recommendations for Multimodality Imaging in Cardiac Amyloidosis: Part 1 of 2—Evidence Base and Standardized Methods of Imaging. J Card Fail 2019;25:e1–39. [PubMed: 31473268]

[4]. Dorbala S, Ando Y, Bokhari S, Dispenzieri A, Falk RH, Ferrari VA, et al. ASNC/AHA/ASE/EANM/HFSA/ISA/SCMR/SNMMI expert consensus recommendations for multimodality imaging in cardiac amyloidosis: Part 2 of 2—Diagnostic criteria and appropriate utilization. J Nucl Cardiol 2019:1–15.

[5]. Lane T, Fontana M, Martinez-Naharro A, Quarta CC, Whelan CJ, Petrie A, et al. Natural History, Quality of Life, and Outcome in Cardiac Transthyretin Amyloidosis. Circulation 2019;140:16–26. [PubMed: 31109193]

[6]. Aimo A, Castiglione V, Rapezzi C, Franzini M, Panichella G, Vergaro G, et al. RNA-targeting and gene editing therapies for transthyretin amyloidosis. Nat Rev Cardiol 2022;19. 10.1038/s41569-022-00683-z.

[7]. Campbell CM, Zhang K, Lenihan DJ, Witteles R. Developing Therapy for Transthyretin Amyloidosis. Am J Med 2022;135. 10.1016/j.amjmed.2022.01.002. [PubMed: 34508703]

[8]. Kyriakou P, Mouselimis D, Tsarouchas A, Rigopoulos A, Bakogiannis C, Noutsias M, et al. Diagnosis of cardiac amyloidosis: A systematic review on the role of imaging and biomarkers. BMC Cardiovasc Disord 2018;18.

[9]. Tzschätzsch H, Hättasch R, Knebel F, Klaua R, Schultz M, Jenderka K-V, et al. Isovolumetric elasticity alteration in the human heart detected by in vivo time-harmonic elastography. Ultrasound Med Biol 2013;39:2272–8. [PubMed: 24035628]

[10]. Keijzer LBH, Strachinaru M, Bowen DJ, Caenen A, Van der Steen AFW, Verweij MD, et al. Parasternal versus Apical View in Cardiac Natural Mechanical Wave Speed Measurements. IEEE Trans Ultrason Ferroelectr Freq Control 2020:1–1.

[11]. Strachinaru M, Bosch JG, van Gils L, van Dalen BM, Schinkel AFL, van der Steen AFW, et al. Naturally Occurring Shear Waves in Healthy Volunteers and Hypertrophic Cardiomyopathy Patients. Ultrasound Med Biol 2019;45:1977–86. [PubMed: 31079873]

[12]. Salles S, Espeland T, Molares A, Aase SA, Hammer TA, Støylen A, et al. 3D Myocardial Mechanical Wave Measurements: Toward In Vivo 3D Myocardial Elasticity Mapping. JACC Cardiovasc Imaging 2020.

[13]. Lo Q, Haluska B, Chia EM, Lin MW, Richards D, Marwick T, et al. Alterations in regional myocardial deformation assessed by strain imaging in cardiac amyloidosis. Echocardiography 2016;33:1844–53. [PubMed: 27600102]

[14]. Bravo PE, Fujikura K, Kijewski MF, Jerosch-Herold M, Jacob S, El-Sady MS, et al. Relative Apical Sparing of Myocardial Longitudinal Strain Is Explained by Regional Differences in Total Amyloid Mass Rather Than the Proportion of Amyloid Deposits. JACC Cardiovasc Imaging 2019;12:1165–73. [PubMed: 30121266]

[15]. Pislaru C, Ionescu F, Alashry M, Petrescu I, Pellikka PA, Grogan M, et al. Myocardial Stiffness by Intrinsic Cardiac Elastography in Patients with Amyloidosis: Comparison with Chamber Stiffness and Global Longitudinal Strain. J Am Soc Echocardiogr 2019;32:958–968.e4. [PubMed: 31230779]

[16]. Kakkad V, LeFevre M, Roy Choudhury K, Kisslo J, Trahey GE. Effect of Transmit Beamforming on Clutter Levels in Transthoracic Echocardiography. Ultrason Imaging 2018;40:215–31. [PubMed: 29683052]

[17]. Kakkad V, LeFevre M, Hollender P, Kisslo J, Trahey GE. Non-invasive Measurement of Dynamic Myocardial Stiffness Using Acoustic Radiation Force Impulse Imaging. Ultrasound Med Biol 2019;45:1112–30. [PubMed: 30890282]

[18]. Keijzer LBHH, Caenen A, Voorneveld J, Strachinaru M, Bowen DJ, Van De Wouw J, et al. A direct comparison of natural and acoustic-radiation-force-induced cardiac mechanical waves. Sci Rep 2020;10. [PubMed: 32001736]

[19]. Pernot M, Couade M, Mateo P, Crozatier B, Fischmeister R, Tanter MM. Real-time assessment of myocardial contractility using shear wave imaging. J Am Coll Cardiol 2011;58:65–72. [PubMed: 21700091]

[20]. Pernot M, Lee WN, Bel A, Mateo P, Couade M, Tanter M, et al. Shear Wave Imaging of Passive Diastolic Myocardial Stiffness: Stunned Versus Infarcted Myocardium. JACC Cardiovasc Imaging 2016;9:1023–30. [PubMed: 27236522]

[21]. Keijzer LBH, Voorneveld J, Bowen DJ, Strachinaru M, Van Der Steen AFW, De Jong N, et al. A comparison of natural and acoustic radiation force induced shear wave propagation speed measurements in open-chest pigs. IEEE Int. Ultrason. Symp. IUS, vol. 2019- Octob, 2019, p. 2110–3.

[22]. Song P, Bi X, Mellema DC, Manduca A, Urban MW, Pellikka PA, et al. Pediatric cardiac shear wave elastography for quantitative assessment of myocardial stiffness: A pilot study in healthy controls. Ultrasound Med Biol 2016;42:1719–29. 10.1016/j.ultrasmedbio.2016.03.009. [PubMed: 27140522]

[23]. Song P, Bi X, Mellema DC, Manduca A, Urban MW, Greenleaf JF, et al. Quantitative assessment of left ventricular diastolic stiffness using cardiac shear wave elastography. J Ultrasound Med 2016;35:1419–27. 10.7863/ultra.15.08053. [PubMed: 27208201]

[24]. Salles S, Lovstakken L, Aase SA, Bjastad TG, Torp H. Clutter Filter Wave Imaging. IEEE Trans Ultrason Ferroelectr Freq Control 2019;66:1444–52. 10.1109/TUFFC.2019.2923710. [PubMed: 31226072]

[25]. Pislaru C, Alashry MM, Thaden JJ, Pellikka PA, Enriquez-Sarano M, Pislaru SV. Intrinsic Wave Propagation of Myocardial Stretch, A New Tool to Evaluate Myocardial Stiffness: A Pilot Study in Patients with Aortic Stenosis and Mitral Regurgitation. J Am Soc Echocardiogr 2017;30:1070–80. 10.1016/j.echo.2017.06.023. [PubMed: 28822668]

[26]. Villemain O, Correia M, Mousseaux E, Baranger J, Zarka S, Podetti I, et al. Myocardial Stiffness Evaluation Using Noninvasive Shear Wave Imaging in Healthy and Hypertrophic Cardiomyopathic Adults. JACC Cardiovasc Imaging 2019;12:1135–45. [PubMed: 29550319]

[27]. Lauer B, Schannwell M, Kühl U, Strauer BE, Schultheiss HP. Antimyosin autoantibodies are associated with deterioration of systolic and diastolic left ventricular function in patients with chronic myocarditis. J Am Coll Cardiol 2000;35:11–8. [PubMed: 10636253]

[28]. Palka P, Macdonald G, Lange A, Burstow DJ. The role of Doppler left ventricular filling indexes and Doppler tissue echocardiography in the assessment of cardiac involvement in hereditary hemochromatosis. J Am Soc Echocardiogr 2002;15:884–90. [PubMed: 12221404]

[29]. Lang RM, Badano LP, Victor MA, Afilalo J, Armstrong A, Ernande L, et al. Recommendations for cardiac chamber quantification by echocardiography in adults: An update from the American Society of Echocardiography and the European Association of Cardiovascular Imaging. J Am Soc Echocardiogr 2015;28:1–39.e14. 10.1016/j.echo.2014.10.003. [PubMed: 25559473]

[30]. Nagueh SF, Smiseth OA, Appleton CP, Byrd BF, Dokainish H, Edvardsen T, et al. Recommendations for the Evaluation of Left Ventricular Diastolic Function by Echocardiography: An Update from the American Society of Echocardiography and the European Association of Cardiovascular Imaging. J Am Soc Echocardiogr 2016;29:277–314. [PubMed: 27037982]

[31]. Rubin J, Steidley DE, Carlsson M, Ong M-L, Maurer MS. Myocardial Contraction Fraction by M-Mode Echocardiography Is Superior to Ejection Fraction in Predicting Mortality in Transthyretin Amyloidosis. J Card Fail 2018;24:504–11. [PubMed: 30010028]

[32]. Jin F, Knight A, Trutna C, Pietrosimone L, Hobson-Webb L, Nightingale K, et al. An Open-Source Radon-Transform Shear Wave Speed Estimator with Masking Functionality to Isolate Different Shear-Wave Modes. IEEE Int. Ultrason. Symp, IEEE; 2022, p. 1–4.

[33]. Vos HJ, van Dalen BM, Heinonen I, Bosch JG, Sorop O, Duncker DJ, et al. Cardiac Shear Wave Velocity Detection in the Porcine Heart. Ultrasound Med Biol 2017;43:753–64. [PubMed: 28065540]

[34]. Petrescu A, Santos P, Orlowska M, Pedrosa J, Bézy S, Chakraborty B, et al. Velocities of Naturally Occurring Myocardial Shear Waves Increase With Age and in Cardiac Amyloidosis. JACC Cardiovasc Imaging 2019.

[35]. Martinez-Naharro A, Baksi AJ, Hawkins PN, Fontana M. Diagnostic imaging of cardiac amyloidosis. Nat Rev Cardiol 2020;17:413–26. [PubMed: 32042139]

[36]. Brenner DA, Jain M, Pimentel DR, Wang B, Connors LH, Skinner M, et al. Human Amyloidogenic Light Chains Directly Impair Cardiomyocyte Function Through an Increase in Cellular Oxidant Stress. Circ Res 2004;94:1008–10. [PubMed: 15044325]

[37]. Bellavia D, Abraham TP, Pellikka PA, Al-Zahrani GB, Dispenzieri A, Oh JK, et al. Detection of Left Ventricular Systolic Dysfunction in Cardiac Amyloidosis with Strain Rate Echocardiography. J Am Soc Echocardiogr 2007;20:1194–202. [PubMed: 17596912]

[38]. Koyama J, Ray-Sequin PA, Falk RH. Longitudinal myocardial function assessed by tissue velocity, strain, and strain rate tissue doppler echocardiography in patients with AL (primary) cardiac amyloidosis. Circulation 2003;107:2446–52. [PubMed: 12743000]

[39]. Pagourelias ED, Mirea O, Duchenne J, Van Cleemput J, Delforge M, Bogaert J, et al. Echo Parameters for Differential Diagnosis in Cardiac Amyloidosis: A Head-to-Head Comparison of Deformation and Nondeformation Parameters. Circ Cardiovasc Imaging 2017;10.

[40]. Papadacci C, Finel V, Villemain O, Tanter M, Pernot M. 4D Ultrafast Ultrasound Imaging of Naturally Occurring Shear Waves in the Human Heart. IEEE Trans Med Imaging 2020;39. 10.1109/TMI.2020.3020147.

[41]. Sabbadini A, Caenen A, Keijzer LBH, van Neer PLMJ, Vos HJ, de Jong N, et al. Tapering of the interventricular septum can affect ultrasound shear wave elastography: An in vitro and in silico study. J Acoust Soc Am 2021;150:428–40. [PubMed: 34340474]

[42]. Fatemi A, Berg EAR, Rodriguez-Molares A. Studying the Origin of Reverberation Clutter in Echocardiography: In Vitro Experiments and In Vivo Demonstrations. Ultrasound Med Biol 2019;45:1799–813. [PubMed: 31053427]

[43]. Santos P, Petrescu AM, Pedrosa JP, Orlowska M, Komini V, Voigt JU, et al. Natural Shear Wave Imaging in the Human Heart: Normal Values, Feasibility, and Reproducibility. IEEE Trans Ultrason Ferroelectr Freq Control 2019;66:442–52. [PubMed: 30442606]

[44]. Kanai H Propagation of spontaneously actuated pulsive vibration in human heart wall and in vivo viscoelasticity estimation. Freq Control IEEE Trans 2005;52.

[45]. Pernot M, Villemain O. In the Heart of Stiffness: Are Natural Heart Vibrations Reliable Enough to Assess Myocardial Stiffness, The New Holy Grail in Echocardiography? JACC Cardiovasc Imaging 2019.

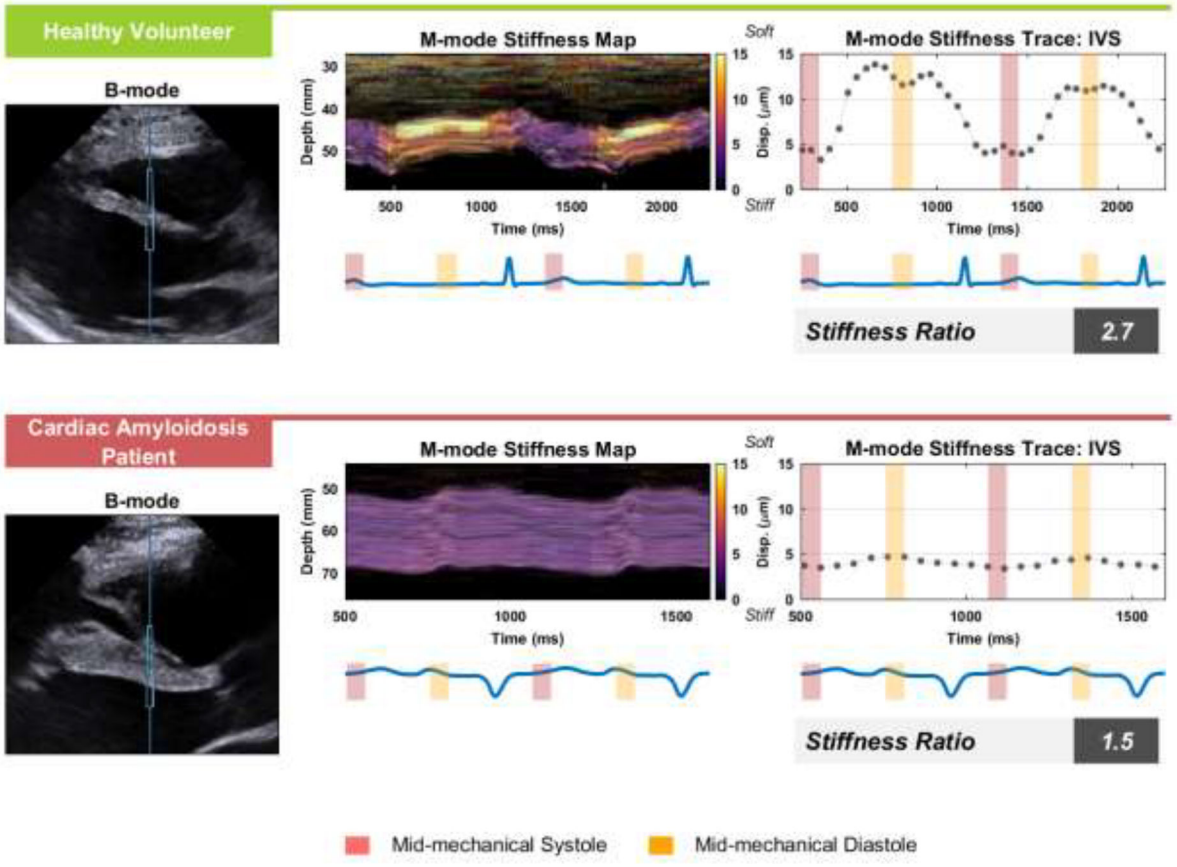

Figure 1: Example ARFI data from a Healthy Volunteer and Cardiac Amyloidosis Patient.

On the left are B-mode images of the parasternal long-axis view of the IVS with the ARFI excitation and ROI marked by the vertical midline and blue box for an example healthy volunteer subject and cardiac amyloidosis patient. In the middle, the M-modes from within the ROI box are shown with a color overlay of the ARFI displacement achieved 1.5 ms after each excitation. Mean ARFI displacement through the septum is shown in right plots, where yellow and red boxes indicate systolic and diastolic periods used for the stiffness ratio, the displacement measured in diastole over the displacement measured in systole. The electrocardiogram is shown beneath both the M-mode and mean displacement plots. ARFI = Acoustic Radiation Force Impulse; IVS = interventricular septum.

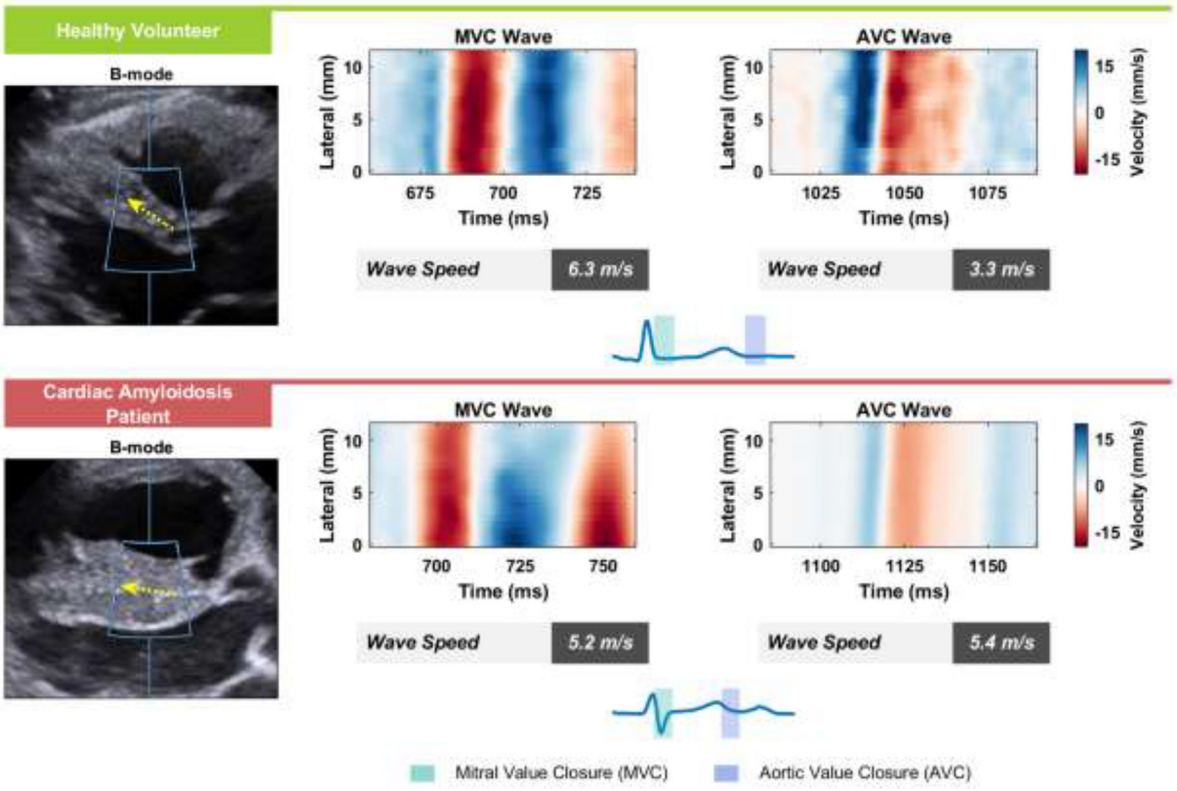

Figure 2: Example Natural Shear Wave Data from a Healthy Volunteer and Cardiac Amyloidosis Patient.

On the left are B-Modes of the parasternal long-axis view of the interventricular septum with the displacement tracking region-of-interest marked by the blue box and the direction of wave propagation indicated by the yellow arrow for an example healthy volunteer subject and cardiac amyloidosis patient. Particle velocity data tracked along the septum containing natural shear waves associated with MVC and AVC are shown. Wave speeds and trajectories (dashed line) were identified using a radon-transform approach. The time intervals corresponding to each natural shear wave are highlighted in the electrocardiograms. AVC = Aortic Valve Closure; MVC = Mitral Valve Closure.

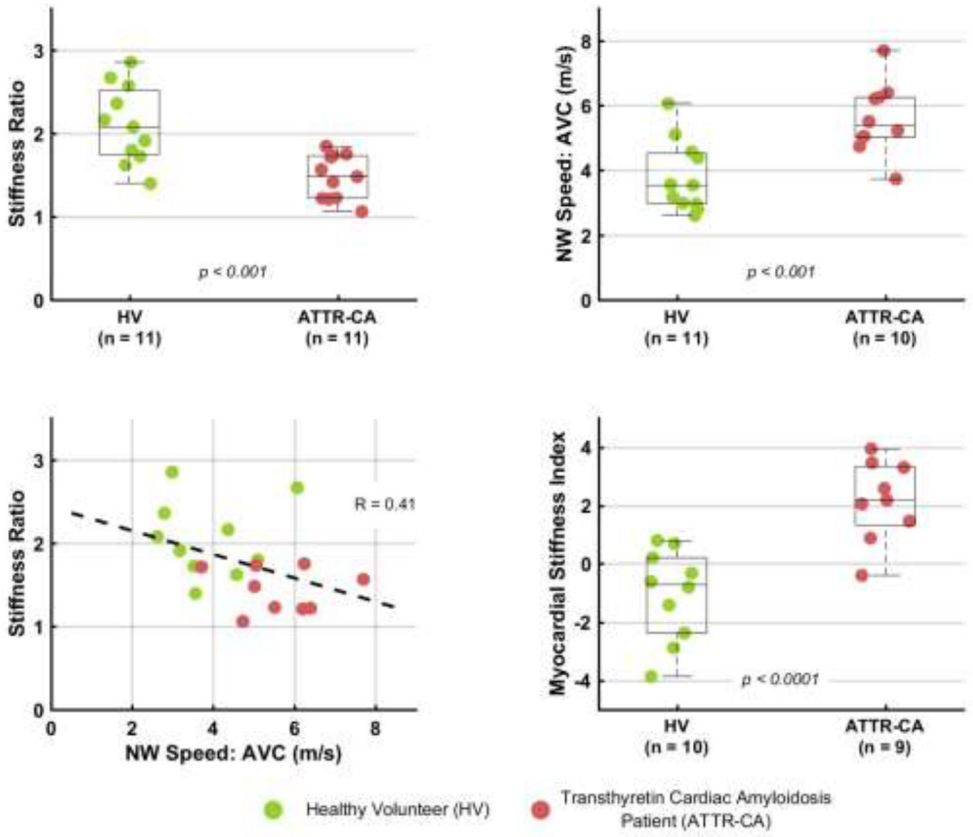

Figure 3: Comparisons of HVs to CA Patients.

HVs are compared to CA patients using the ARFI stiffness ratio in the top left boxplot and the NSW speed in the top right plot. Both metrics are able to separate the groups with statistically significant difference. The bottom left plot shows the weak correlation between stiffness ratio and NSW speed. The bottom right boxplot compares HVs and CA patients using the proposed myocardial stiffness index that combines ARFI and NSW measurements. ARFI = Acoustic Radiation Force Impulse; CA = Cardiac Amyloidosis; HV = Healthy Volunteer; NSW = Natural Shear Wave.

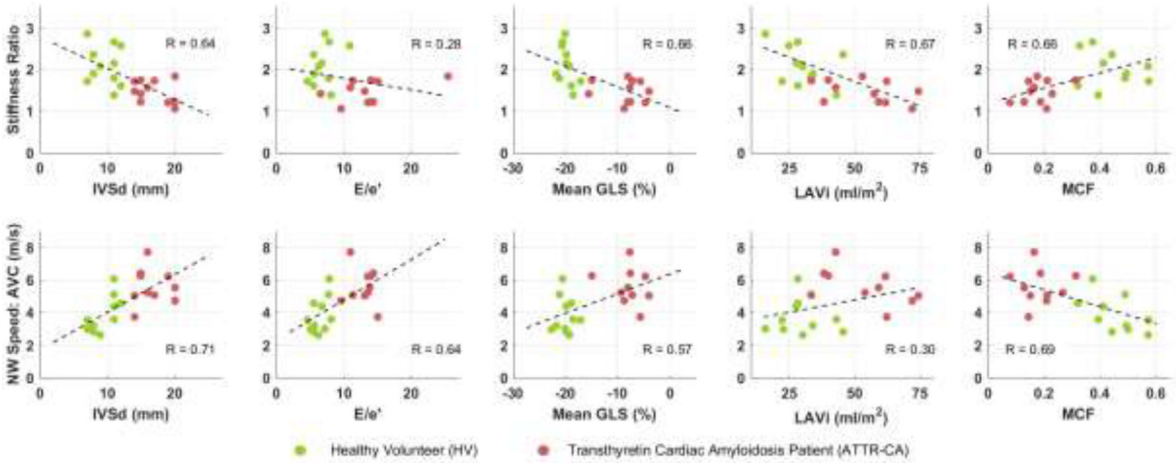

Figure 4: Correlations to Existing Metrics.

ARFI stiffness ratio (upper) and NSW speed (lower) plotted against echocardiography metrics associated with CA (IVSd, E/e', GLS, LAVi, MCF). Dotted line shows linear fit and r^2 shows degree of correlation.

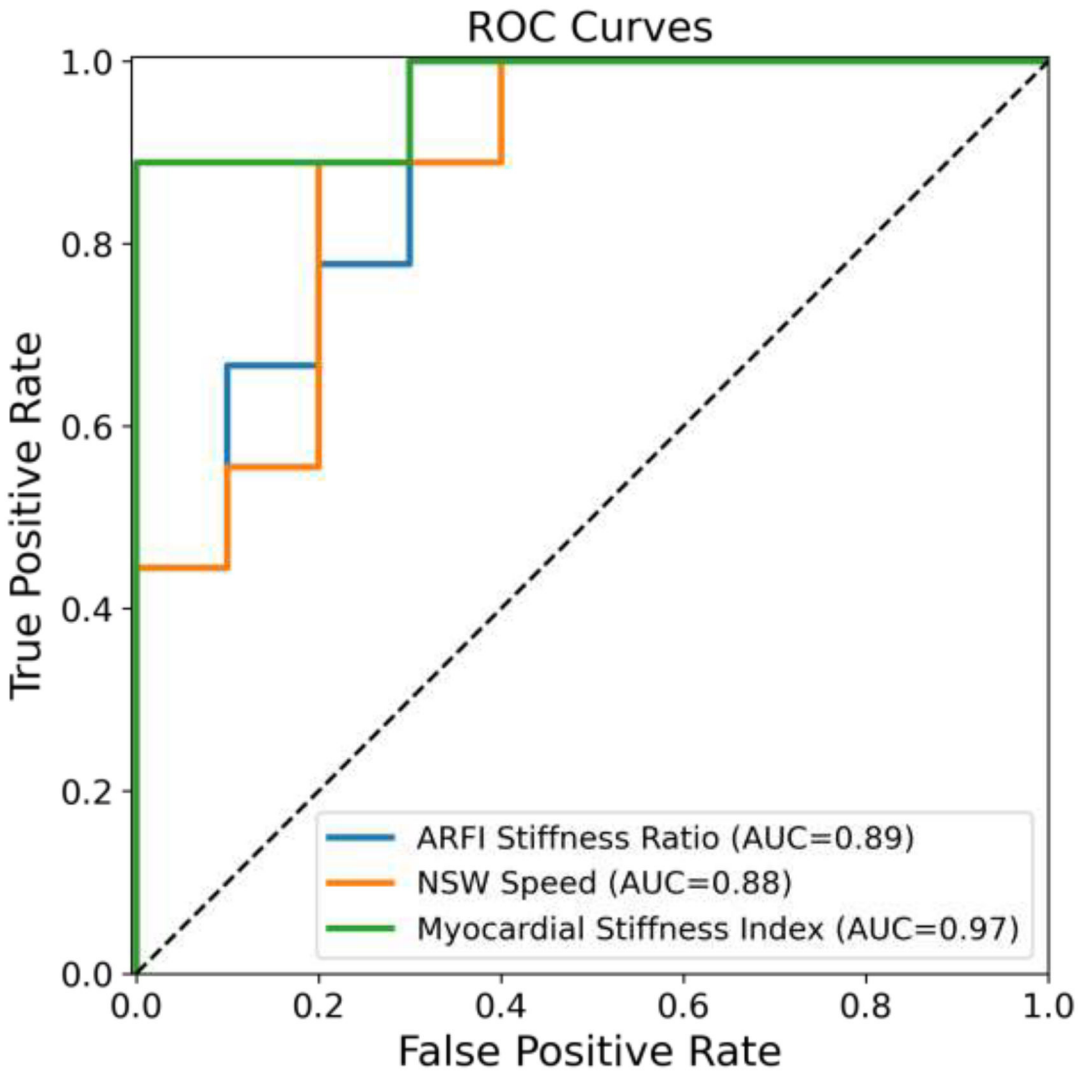

Figure 5: ROC Curves.

Receiver operating characteristic (ROC) curves for ARFI stiffness ratio, NSW speed, and Myocardial Stiffness Index in discriminating CA patients from healthy volunteers. Areas under the curve are listed in the legend.

Table 1:

Population Characteristics

	HV Group (n = 12)	CA Group (n = 13)	p Value
Age, years	57.6 ± 6	72.7± 6.2	<0.001
Sex, M/F	3/12	8/5	<0.001
Race	W/C (8) B/AA (1) Asian (1) Multiracial (1) Other (1)	W/C (1) B/AA (10) Asian (1) Unknown (1)	
Weight, kg	69.3 ± 11.3	82.9 ± 21.2	0.057
Height, cm	164.8 ± 7.1	172.1 ± 11.7	0.069
BSA, m^2	1.76 ± 0.2	1.95 ± 0.3	0.054
BMI, kg/m^2	25.4 ± 3.2	27.6 ± 5	0.027
Systolic BP, mm Hg	129.8 ± 16.6	118.2 ± 19.9	0.126
Diastolic BP, mm Hg	78.3 ± 11	71.4 ± 12.9	0.164
Heart rate, beats/min	64.8 ± 7.1	75.5 ± 12	0.013

Values are mean ± SD or n/n

W/C = White or Caucasian; B/AA = Black or African American; BMI = body mass index; BP = blood pressure; BSA = body surface area; CA = Cardiac Amyloidosis; HV = Healthy Volunteer.

Table 2:

Echocardiography-derived Cardiac Metrics

	HV Group (n = 12)	CA Group (n = 13)	p Value
IVSd, cm	0.95 ± 0.20	1.67 ± 0.23	<0.001
IVSs, cm	1.30 ± 0.15	1.80 ± 0.23	<0.001
PWd, cm	0.91 ± 0.15	1.60 ± 0.21	<0.001
PWs, cm	1.30 ± 0.19	1.80 ± 0.15	<0.001
LV Peak E-wave, cm/s	65.5 ± 10.6	73.5 ± 16.9	0.169
LV Peak A-wave, cm/s	63.1 ± 13.9	51.1 ± 24.2	0.234
Septal Wall e', cm/s	8.4 ± 1.5	4.5 ± 1.3	<0.001
Lateral Wall e', cm/s	11.5 ± 2.9	6.5 ± 1.5	<0.001
E/e'	6.7 ± 1.7	14.1 ± 4.9	<0.001
LV E/A	1.1 ± 0.3	1.7 ± 1.2	0.165
LV DT, ms	210.8 ± 46.0	178.2 ± 44.9	0.087
LV IVCT, ms	64.2 ± 14.7	107.2 ± 76.3	0.068
LV IVRT, ms	77.9 ± 15.3	74.9 ± 23.8	0.710
LV GLS (%)	−20.0 ± 1.5	−8.3 ± 3.4	<0.001
LV EF (%)	59.4 ± 3.6	39.7 ± 14.2	<0.001
LA VI, ml/m^2	29.6 ± 8.4	54.0 ± 13.2	<0.001
LA VI > 34 ml/m^2	2/11 (18%)	11/13 (84%)	
LV Mass, g	127.4 ± 22.9	286.6 ± 77.6	<0.001
LV Mass Index, g/m^2	72.2 ± 9.4	145.8 ± 27.7	<0.001
MCF	0.47 ± 0.13	0.19 ± 0.06	<0.001
Diastolic Grade	Normal (10) Indeterminate (2)	Indeterminate (6) Grade 1 (1) Grade 2 (3) Grade 3 (3)	

Values are mean ± SD, n/n (%)

A = late mitral inflow velocity; CA = cardiac amyloidosis; DT = deceleration time; E = early mitral inflow velocity; e' = early mitral annular velocity; EF = ejection fraction; GLS = global longitudinal strain; HV = healthy volunteer; IVCT = isovolumic contraction time; IVRT = isovolumic relaxation time; IVS = interventricular septum; IVSd = IVS thickness at end-diastole; IVSs = IVS thickness at end-systole; LA = left atrium; LV = left ventricle; MCF = myocardial 34 contraction factor; PW = posterior wall; PWd = PW thickness at end-diastole; PWs = PW thickness at end-systole; VI = volume index.

Table 3:

Correlation Between Echocardiography Metrics with Stiffness Ratio, Natural Shear Wave Speed, and Myocardial Stiffness Index.

	ARFI Stiffness Ratio Correlation Coefficient, (R)	Natural Wave Speed Correlation Coefficient, (R)	Myocardial Stiffness Index Correlation Coefficient, (R)
IVSd	−0.73*	0.68*	0.84*
IVSs	−0.77*	0.65*	0.85*
PWd	−0.58*	0.51*	0.65*
PWs	−0.63*	0.63*	0.75*
LVIDd	−0.27	−0.03	0.14
LVIDs	−0.58*	0.24	0.48*
E	−0.03	0.09	0.06
A	0.19	−0.26	−0.27
E/e’	−0.53*	0.61*	0.68*
E/A	−0.16	0.35	0.32
DT	0.27	0.05	−0.14
MCOT	0.10	−0.17	−0.19
LVET	0.31	−0.34	−0.39
IVCT	−0.24	0.11	0.20
IVRT	0.32	−0.14	−0.27
GLS Average	−0.67*	0.53*	0.71*
EFBiplane	0.59*	−0.34	−0.55*
EDV	−0.48*	0.08	0.32
ESV	−0.54*	0.19	0.43
SV	0.14	−0.27	−0.28
LA Volume	−0.70*	0.32	0.59*
LA Volume Index	−0.65*	0.25	0.53*
LV Mass	−0.71*	0.49*	0.71*
LV Mass Index	−0.71*	0.49*	0.71*

MCOT = mitral valve closure-to-opening time; LVET = left ventricle ejection time; other abbreviations as in Table 2.

* indicates that the correlation is statistically significant with $p<0.05$

Table 4:

Diagnostic Utility of Stiffness Ratio, NSW Speed, and Myocardial Stiffness Index.

	Stiffness Ratio	NSW Speed	Myocardial Stiffness Index
Sensitivity (%)	90.9%	90%	88.9%
Specificity (%)	72.7%	81.8%	100%
Optimal Cutoff Value	1.79	4.57 m/s	0.12
AUC [95% CI]	0.89 [0.70, 1.0]	0.88 [0.71, 1.0]	0.97 [0.87, 1.0]